Large unidirectional magnetoresistance from the dual functionality of copper oxide in naturally oxidized light-metal Al/Cu bilayer films

Lijuan Zhao, Yuzhi Li, Fu Liu, Tong Li, Yongzuo Wang, Xu Liu, Dezheng Yang, Changjun Jiang, and Cunxu Gao*

Key Laboratory for Magnetism and Magnetic Materials of the Ministry of Education, Lanzhou University, Lanzhou 730000, People's Republic of China

(Received 15 November 2023; revised 31 January 2024; accepted 20 March 2024; published 9 April 2024)

Unidirectional magnetoresistance (UMR) has garnered extensive attention for its rich physics and potential applications. The prevailing belief is that indispensable ferromagnetic films serve as scattering sources of polarized electrons or that noncentrosymmetric systems cause spin band splitting, driving most research toward ferromagnet/normal-metal bilayer films or nonmagnetic Rashba systems. However, our observations reveal a significant UMR in bilayer films consisting solely of the oxidized light metal Al/Cu. Remarkably, the UMR signal of 0.073% is approximately one order of magnitude larger than that of most structures. Such a UMR is attributed to the dual functionality of copper oxide, which not only generates polarized electrons—a recognized function—but also scatters these electrons in a weak magnetization manner. Our findings provide a fresh strategy to generate the UMR, facilitating its application through the use of more readily available materials.

DOI: 10.1103/PhysRevApplied.21.044020

I. INTRODUCTION

Unidirectional magnetoresistance (UMR) has sparked a surge of interest in probing spin states by two-terminal planar devices that are simpler than the three-terminal geometry of magnetic tunnel junctions [1–3] and preparing rectification and logic devices [4–6] due to its unidirectional nature. In common magnetoresistance effects like anisotropic magnetoresistance [7] and spin Hall magnetoresistance (SMR) [8,9], the resistance remains invariant regardless of flipping upside down in the current density **J** or magnetization **M** direction. Conversely, the sign of UMR varies in response to the **J** or **M** direction flipping, signifying a unidirectional or nonreciprocal feature [1–3,10–23].

The emergence of UMR can originate from spin-dependent scattering, magnon excitation [2,20,21], and the spin-orbit torque (SOT) effect [3,11,17,19,24]. Thus generating a large spin current by strong spin-orbit coupling (SOC) materials is considered as an essential factor. This fact has led, in the past few years, to extensive efforts having been made in heavy-metal/ferromagnet (HM/FM) bilayer films [1–3,10–13,25,26]. Meanwhile, UMR is also attributed to the modulation of Rashba-type spin band splitting by an applied magnetic field [4,5,27–30]. As a result, nonmagnetic noncentrosymmetric Rashba systems with a large Rashba SOC have also been extensively studied, examples of which include polar semiconductors [4,28] and interface/surface Rashba systems [30]. Within the origin of UMR, the necessity for strong SOC limits the kinds of suitable materials in two-terminal devices.

Recently, UMR has been observed in naturally oxidized light-metal copper/ferromagnet (CuO_x/FM) bilayer films, even in the presence of negligible SOC. In addition to the common thermoelectric effect [31–39], two different mechanisms have been proposed to elucidate this occurrence [31,32]. Okano *et al.* demonstrate the spin-dependent scattering leading to UMR, as depicted in Fig. 1(a), where the spin current is generated by spin-vorticity coupling due to a strong gradient of electrical mobility in CuO_x [31]. Alternatively, Ding *et al.* attribute the UMR to orbital-dependent electron scattering and orbital-spin conversion, as illustrated in Fig. 1(b), called orbital UMR, where the orbital current is driven by the orbital Rashba-Edelstein effect [32]. In both proposed mechanisms, an essential adjacent FM (either Co or FeNi) serves as the scattering source or absorber of polarized electrons, while CuO_x acts solely as the generator of polarized current.

Similarly, CuO_x with the same function has also been extensively utilized in recent orbital torque studies [40–47]. However, magnetic measurements on naturally oxidized 3-nm-thick copper, as well as anomalous Hall resistance on naturally oxidized Al/Cu bilayer films, have revealed that CuO_x itself possesses a weak magnetic moment [48,49]. This discovery has prompted a fresh question in physics: Can CuO_x effectively serve a dual functionality—providing polarized angular momentum while also scattering this angular

*Corresponding author. gaocunx@lzu.edu.cn

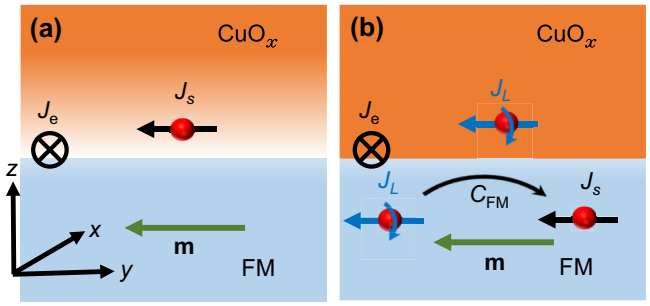

FIG. 1. Illustration of spin-dependent UMR (a) and orbital-dependent UMR (b). Black arrows and blue arrows with circles represent the spin current generated by the bulk of CuO_x and the orbital current generated by the CuO_x/FM interface, respectively. The green arrows indicate the magnetic moment of the FM. Finally, C_{FM} denotes the SOC of the FM, transforming orbital currents into spin currents.

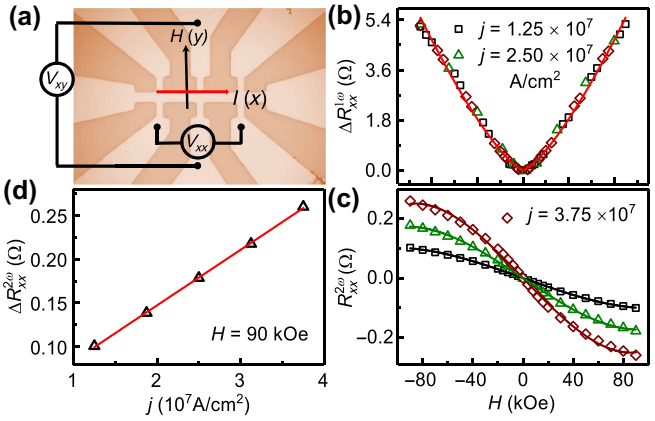

FIG. 2. (a) Schematic diagram of the $R_{xx}^{1\omega}$ and $R_{xx}^{2\omega}$ measurement geometry. (b) Dependence of magnetic field H on the magnitude of the first-harmonic longitudinal resistance $\Delta R_{xx}^{1\omega} = R_{xx}^{1\omega}(H) - R_{xx}^{1\omega}(H{=}0)$ in Al(3 nm)/Cu(1.6 nm) heterostructures recorded under different current densities. (c) The second-harmonic longitudinal resistance $R_{xx}^{2\omega}$ as a function of H. The solid lines in (b) and (c) represent the fitting results using $R_{xx}^{1\omega} = bH^n$ and $R_{xx}^{2\omega} = cH + dH^3$, respectively, where b, c, and d are undetermined parameters. (d) Linear fit of the current-density dependence on the magnitude of the second-harmonic resistance $[\Delta R_{xx}^{2\omega} = |(R_{xx}^{2\omega}(H,j) - R_{xx}^{2\omega}(-H,j))|/2]$.

momentum—thus potentially imitating the UMR effect? The absence of experiment may hinder our advancement in understanding and harnessing the UMR effect.

In this paper, we achieve the UMR effect by constructing naturally oxidized light-metal Al/Cu bilayer films without an adjacent designed FM such as FeNi or Co. We found that the UMR ratio of 0.073% is one order of magnitude larger than that of CuO_x/FM bilayer films. The temperature dependence of UMR signals in oxidized Al/Cu bilayer and contrasting Al/Cu/Co trilayer films indicates magnetically correlated scattering and excludes the contribution of structural inversion asymmetry with Rashba SOC. We attribute the UMR to the dual functionality of copper oxide. On the one hand, it yields polarized electrons, while, on the other hand, it possesses a weak magnetic moment. It results in interfacial scattering occurring between the polarized electrons and the magnetic moment.

II. EXPERIMENT

The Al/Cu bilayer and Al/Cu/Co trilayer films were grown on Si substrates by a molecular beam epitaxy (MBE) system with a base pressure of 10^{-10} mbar. In these heterostructures, the thicknesses of both the Al and Cu films were systematically varied in order to tune the depth of the copper oxides and reduce the shunting in the copper. Hall bar devices with a width of 10 μm and maximum aspect ratio of ∼8 were patterned by photolithography and liftoff. The devices were stored in air for 5 days to naturally oxidize before the transport measurements (detailed sample fabrication and oxidation characterization are as shown in Ref. [49]).

To measure the UMR, we used the technique of second-harmonic longitudinal and transverse voltage at different temperatures, where an in-plane alternating current with frequency $\omega = 133$ Hz was applied. The spin-torque ferromagnetic resonance (ST-FMR) measurements were carried out by injecting a 30 dBm microwave current of 8–12 GHz, at an angle of 45° with the magnetic field direction, into the oxidized Al/Cu/Co trilayer films.

III. UMR CHARACTERIZATION

In the UMR measurement, an alternating current was applied along the x axis of the Hall bar, while a scanning magnetic field, reaching up to 90 kOe along the y axis, was employed as shown in Fig. 2(a). The results of the first- and second-harmonic longitudinal resistances are shown in Figs. 2(b) and 2(c), respectively. The magnitude of the first-harmonic longitudinal resistance $\Delta R_{xx}^{1\omega}$ remains unaffected by the current density, whereas the second-harmonic longitudinal resistance $R_{xx}^{2\omega}$ exhibits a notable dependence on the current density. Figure 2(d) shows the linear fitting results for $\Delta R_{xx}^{2\omega}$ at an example magnetic field of 90 kOe (red line). This behavior aligns with that of the known UMR in ferromagnet/normal-metal (FM/NM) bilayer films [3,11,12].

By subjecting $R_{xx}^{1\omega}$ and $R_{xx}^{2\omega}$ data to a fitting analysis against the magnetic field H, we discerned that, in oxidized Al/Cu, $\Delta R_{xx}^{1\omega}$ follows a power-law relation of the form bH^n, consistent with the classical magnetoresistance described by Kohler's rule [50]. In contrast, $R_{xx}^{2\omega}$ exhibits a dependence on $cH + dH^3$, a pattern that aligns with the responsiveness of the magnetic moment to the applied H [Appendix A, Fig. 5(a)]. This behavior stands in contrast to what is typically observed in HM/FM bilayer films, where

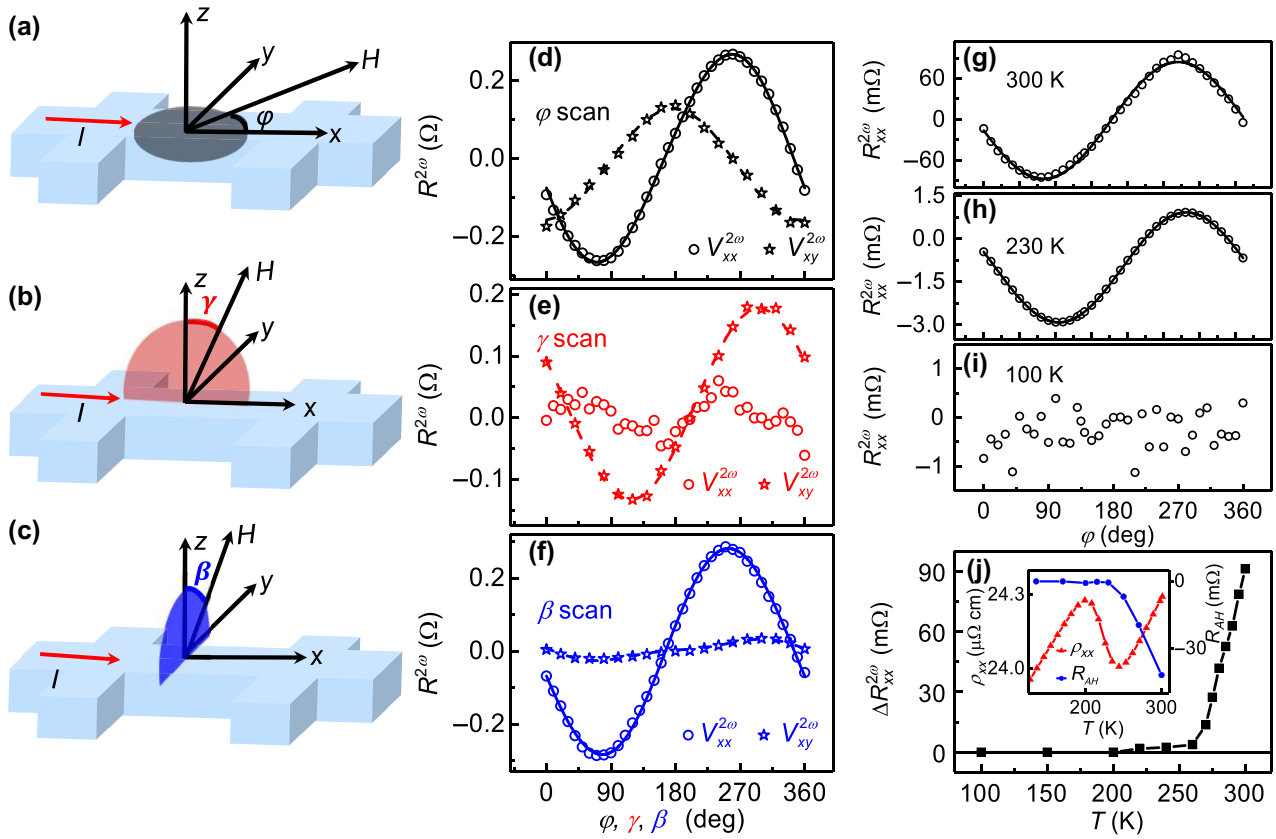

FIG. 3. (a)–(c) Geometries of the measurements and definitions of rotation planes. (d)–(f) The angular dependence of the second-harmonic longitudinal $R_{xx}^{2\omega}$ and transverse $R_{xy}^{2\omega}$ resistance measured in the (d) φ, (e) γ, and (f) β rotation planes with a current density of $j = 3.75 \times 10^7$ A/cm^2 at 300 K. (g)–(i) Plots showing φ scans of $R_{xx}^{2\omega}$ at (g) 300 K, (h) 230 K, and (i) 100 K. (j) Plot of $\Delta R_{xx}^{2\omega}$ as a function of the temperature measured at $H = 90$ kOe and $j = 1.25 \times 10^7$ A/cm^2. The inset displays the temperature dependence of the resistivity ρ_{xx} and anomalous Hall resistance R_{AH} for the Al(3 nm)/Cu(1.6 nm) bilayer films.

$R_{xx}^{2\omega}$ manifests a dependence on H^{-p} in a multidomain state and remains independent of H in a single-domain state [2].

Furthermore, the angular dependence of UMR was studied by rotating the direction of the applied magnetic field H in the xy plane (φ scan), the zx plane (γ scan), and the zy plane (β scan). Schematic illustrations of the measurement configurations for angular dependence are shown in Figs. 3(a)–3(c) with H set to 90 kOe. As shown in Figs. 3(d)–3(f), $R_{xx}^{2\omega}$ follows $\sin\varphi$ and $\sin\beta$ functions in the φ and β scans at a current density of $j = 3.75 \times 10^7$ A/cm^2 and a temperature of 300 K. However, $R_{xx}^{2\omega}$ is zero in the γ scan.

Such a symmetry of $\sin\varphi$ ($\sin\beta$) is consistent with UMR observed in HM/FM and CuO_x/FM bilayer films, which is commonly attributed to spin- and orbital-dependent scattering, spin-flipping UMR (SF-UMR), thermal effects, and SOT. The SF-UMR originates from the generation and annihilation of magnons. Its characteristic feature is a sharp increase in UMR with a small incremental rise at low magnetic field [2]. On the other hand, the SOT effect stems from the manipulation of the magnetic moment of FM by an equivalent magnetic field generated by the spin current. This effect is characterized by a decrease in UMR value as the magnetic field increases. In oxidized Al/Cu bilayer films, the SF-UMR and SOT effects are absent due to the slow increase of UMR with the magnetic field across the entire field range in Fig. 2(c). In the following, we discuss whether spin- and orbital-dependent scattering and thermal effects occur in oxidized Al/Cu bilayer films without an artificially designed FM.

IV. THERMAL EFFECTS

Related thermoelectric effects, including the anomalous (normal) Nernst effect [33,36–38] and spin Seebeck effect [39], are analyzed, which exhibit similar angular dependence as observed for $R^{2\omega}$. Typically, temperature gradients are created due to the inhomogeneity of the resistivity such as two heterojunctions with different resistivities. Assuming a sample with vertical thermal gradients, the longitudinal and transverse magnetoresistances can be expressed as follows: $R_{xx}^{2\omega} = \alpha \nabla T_z l l M(H) \sin\beta \sin\varphi$ and $R_{xy}^{2\omega} = \alpha \nabla T_z I w M(H) \sin\gamma \cos\varphi$. Here l and w denote the

length and width of the Hall bar, respectively, and I, M and α are the magnitudes of the charge current, magnetization, and a constant, respectively. These equations explicitly convey that the ratios of $R_{xx}^{2\omega}$ and $R_{xy}^{2\omega}$ are contingent upon the proportions of the Hall bar's length and width.

Experimental measurements of $R_{xy}^{2\omega}$, as shown in Figs. 3(d)–3(f), evince a symmetry of $\sin\gamma\cos\varphi$, aligning with the theoretical formulation for the thermal effect. The aspect ratio of the Hall bar ($l/w = 80\ \mu\text{m}/10\ \mu\text{m} = 8$) surpasses the magnitude of the ratio

$$\frac{R_{xx}^{2\omega}(H = 90\ \text{kOe}, j = 3.75 \times 10^7\ \text{A/cm}^2, \varphi = 90^\circ)}{R_{xy}^{2\omega}(H = 90\ \text{kOe}, j = 3.75 \times 10^7\ \text{A/cm}^2, \varphi = 0^\circ)}$$

in Fig. 3(d), approximately 1.67. This suggests that the UMR exhibits a sign opposite to that of thermal resistance, a phenomenon similar to that reported in thin CoPt films with a positive Co gradient [13], thin CoCr/Pt bilayer films [2], and monocrystalline Fe/Pt bilayer films [16]. Consequently, although thermal effects exert an influence, they are not the primary determinant; rather, other concurrent factors contribute significantly to the observed UMR effect.

After taking into account the thermal effect and the shunting effect (see Appendix B), we obtain a large ratio $R_{xx}^{\text{UMR}}/R_{\text{AlO}_x/\text{CuO}_x+\text{CuO}_x}$ of 0.073% in oxidized Al(3 nm)/Cu(1.6 nm) bilayer films, where

$$\begin{aligned} R_{xx}^{\text{UMR}} &= R_{xx}^{2\omega}(H = 90\ \text{kOe}, j = 3.75 \times 10^7\ \text{A/cm}^2, \varphi = 90^\circ) \\ &\quad - 8R_{xy}^{2\omega}(H = 90\ \text{kOe}, j \\ &= 3.75 \times 10^7\ \text{A/cm}^2, \varphi = 0^\circ) \end{aligned}$$

and $R_{\text{AlO}_x/\text{CuO}_x+\text{CuO}_x}$ is the combined resistance of the CuO_x layer and the $\text{AlO}_x/\text{CuO}_x$ interface in oxidized Al(3 nm)/Cu(1.6 nm) bilayer films at zero magnetic field. Notably, at a comparable current density as shown in Table I, this ratio is one order of magnitude larger than what has been reported previously for oxidized light-metal/FM including CuO_x/FeNi [31] and CuO_x/Co [32], HM/FM containing W/Co [10], Pt/Co [15], and Ta/Co [24], HM/antiferromagnet of $\text{Pt}/\text{Fe}_2\text{O}_3$ [51] and Pt/FeRh [52] bilayer films, and single FM films such as CoFeB and FeNi [17]. It is found that the greater UMR effect in topological insulator heterojunctions is limited to low temperatures, which is unfavorable for applications [53,54]. Note that, in comparison to the observed UMR effect in W/CoFeB bilayer films (0.36%) [18], the oxidized Al/Cu heterostructure, devoid of heavy metals, presents a more straightforward sample configuration relying on conventional elemental constituents. This renders it better suited for practical applications.

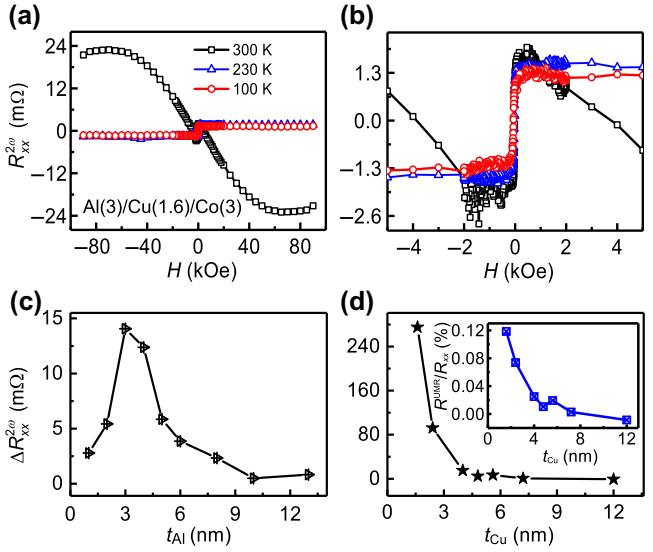

FIG. 4. (a) Field dependence of $R_{xx}^{2\omega}$ for Al(3 nm)/Cu(1.6 nm)/Co(3 nm) trilayer films at different temperatures. The applied H is parallel to the y axis and the current density is $1.74 \times 10^7\ \text{A/cm}^2$. (b) Detail of $R_{xx}^{2\omega}$ in the low-magnetic-field region in panel (a). (c),(d) The UMR as a function of the thickness of the Al (c) and Cu (d) layers at a temperature of 300 K and a magnetic field of 90 kOe. The inset in panel (d) shows the Cu thickness dependence of the ratio of the second to the first harmonic in the φ scan at 300 K.

V. TEMPERATURE-DEPENDENT INTERFACIAL SCATTERING

Spin- and orbital-dependent scattering modulated the interface resistance between the FM and NM due to the accumulation of polarized electrons, which depends on their polarization orientation relative to magnetization. In this scenario, the accumulation of polarized electrons and magnetic moments are identified as crucial factors. Given that the magnetic moment of CuO_x in oxidized Al/Cu bilayer films exhibits significant temperature dependence [Fig. 5(b) in Appendix A], it suggests that the UMR effect in oxidized Al/Cu bilayer films will be an interfacial phenomenon with a pronounced temperature sensitivity.

To validate this analysis, UMR measurements were conducted at different temperatures for an oxidized Al(3 nm)/Cu(1.6 nm) sample, employing a magnetic field of 90 kOe and a current density of $j = 1.25 \times 10^7\ \text{A/cm}^2$. As depicted in Figs. 3(g)–3(i), reducing the temperature from 300 to 200 K results in a 36-fold decrease in $R_{xx}^{2\omega}$. Further lowering the temperature to 100 K leads to a complete suppression of $R_{xx}^{2\omega}$. Figure 3(j) portrays the variation of $\Delta R_{xx}^{2\omega}$ with temperature. The pivotal point around 200 K aligns with the onset of the anomalous Hall effect, the resistivity kink (as shown in the inset), and the zero-field cooling to field cooled bifurcation point in Fig. 5(b). This

TABLE I. Comparison of the UMR magnitude for various material systems (RT = room temperature).

Sample structures	J (A/cm^2)	Conditions	Resistance (Ω)	UMR ratio (%)	Reference
$AlO_x/(CuO_x+Cu)$	3.75×10^7	90 kOe, 300 K	1695	0.073	This work
CuO_x/FeNi	2.5×10^6	0.5 kOe, RT	···	0.00007	[31]
CuO_x/Co	4.0×10^7	5 kOe, RT	120	0.0031	[32]
W/Co	1.0×10^7	17 kOe, RT	570	0.0025	[24]
Pt/Co	1.0×10^7	10 kOe, RT	176	0.0007	[15]
Ta/Co	1.0×10^7	10 kOe, RT	574	0.004	[24]
W/CoFeB	1.67×10^7	0.6 kOe, RT	···	0.36	[18]
CoFeB	1.0×10^7	0.1 kOe, RT	2167	0.00368	[17]
FeNi	1.0×10^7	0.1 kOe, RT	639	0.00391	[17]
Fe_2O_3/Pt	1.0×10^{10}	50 kOe, RT	110	0.026	[51]
FeRh/Pt	1.4×10^7	120 kOe, 10 K	200	0.009	[52]
GaMnAs/BiSb	1.5×10^6	0.2 kOe, 30 K	6750	1.1	[53]
CBST/BST	5.0×10^3	0.7 kOe, 4 K	14 000	0.41	[54]

underscores the direct correlation between the emergence of UMR and the magnetic characteristics of CuO_x.

To establish that the pronounced temperature sensitivity of the UMR is independent of changes in polarized electrons, we conducted a comprehensive measurement of its temperature dependence by combining the UMR and SOT effects. We grew a similar Al(3 nm)/Cu(1.6 nm)/Co(3 nm) heterostructure using MBE and allowed it to oxidize naturally in air. Subsequently, we measured its UMR effect at various temperatures. The data present two discernible features, as depicted in Fig. 4(a).

Above 50 Oe, $R_{xx}^{2\omega}$ is dominated by a constant term that is independent of H at 100 and 230 K, while increasing to near saturation as the magnetic field increases to 90 kOe at 300 K. The increasing $R_{xx}^{2\omega}$ in high magnetic field originates from the oxidized Al(3 nm)/Cu(1.6 nm) interface in oxidized Al(3 nm)/Cu(1.6 nm)/Co(3 nm) trilayer films, which is consistent with the results of Al(3 nm)/Cu(1.6 nm) bilayer films. The observed $\Delta R_{xx}^{2\omega}$ (21.53 mΩ) in oxidized Al(3 nm)/Cu(1.6 nm)/Co(3 nm) trilayer films is one-sixth of that in oxidized Al(3 nm)/Cu(1.6 nm) bilayer films (130.83 mΩ) at $j = 1.74 \times 10^7$ A/cm^2 and $H = 90$ kOe. This significant reduction is attributed to the synergy of the primary shunting effect in the Co layers and the non-negligible contribution from the CuO_x/Co structure (see Appendix B).

Below 50 Oe, on the other hand, $R_{xx}^{2\omega}$ experiences abrupt increments, reaching a plateau, in conjunction with the saturation of the magnetic moment of the Co layers [Appendix A, Fig. 5(c)] at all temperatures, as shown in Fig. 4(b). This conforms to previously reported unidirectional orbital magnetoresistance in oxidized Cu/Co bilayer films [32], where $\Delta R_{xx}^{2\omega}/jR_{\mathrm{Co}}^{1\omega} \approx 1.25 \times 10^{-17}$ A^{-1} m^2. This value closely aligns with the obtained value of 1.81×10^{-17} A^{-1} m^2 in our bilayer films. The persistence of the UMR effect below 50 Oe, even as temperatures decrease to 100 K, suggests that the generation of polarized electrons remains intact.

Furthermore, we conducted quantitative measurement of the efficiency of generating polarized electrons by using the ST-FMR technique (Appendix C). Figure 7(f) shows an enhancement in efficiency below 200 K, signifying an increase in polarized electrons as the temperature is reduced from 200 to 100 K. The increasing efficiency is consistent with that in oxidized $Cu/Ni_{81}Fe_{19}$ bilayer films [55]. These results provide compelling evidence that polarized electrons are not the underlying cause of the disappearance of UMR below 200 K in oxidized Al/Cu bilayer films. Conversely, it can result from the occurrence of the new mechanisms due to antiferromagnetic order of CuO_x, which may necessitate further investigation. Alternatively, we also noted that, at 220 K, fluctuation of the magnetization does not lead to a significant enhancement of the UMR because of the relatively small spin Hall angle at this temperature.

Conventionally, the temperature-dependent UMR can also originate from cooperative interaction between Rashba spin-orbit interaction due to broken inversion symmetry and further breaking time inversion symmetry via applying a magnetic field H [4–6,27–30]. In our samples, Rashba SOC can be negligible by previous investigations on SOT in Al_2O_3/Cu/FM trilayer and CuO_x/FM bilayer films. Instead, there are two possible ways to generate a polarized current. One is orbital current originating from the orbital Rashba-Edelstein effect at the oxidized Al/Cu interface, and the other is spin current resulting from the copper oxide's own mobility gradient [31,32,42]. Additionally, this interaction can induce the UMR effect only on the longitudinal side, while the resistance on the transverse side was also observed in our experiments. More importantly, in the theoretical analysis, the magnitude of UMR depends on the Rashba field λ, the position of the Fermi

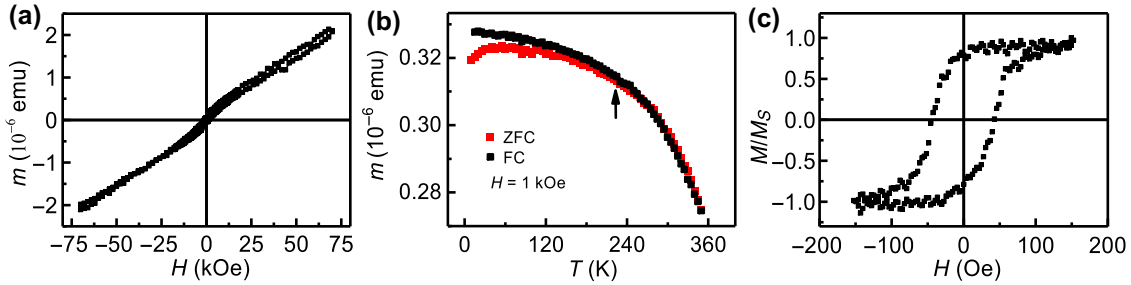

FIG. 5. (a) The m vs H curve of the oxidized Al(2 nm)/Cu(4 nm) bilayer films in an in-plane H configuration on Si substrate. (b) Temperature dependence of the zero-field cooling and field cooled magnetic moment m_{tot} in an in-plane configuration. (c) The hysteresis loop of the oxidized Al(3 nm)/Cu(1.6 nm)/Co(3 nm) trilayer films.

energy μ, and the relaxation time of the electrons τ in the system [4,5,28,30]. We found that only a drastic change in μ (moving from the first to the third region as the temperature decreases) may cause the UMR to disappear [4,28]. According to the above experimental results, the polarized electrons remain increasing below 200 K, suggesting that μ is still in the first or second region. These facts indicate that Rashba spin-orbit interaction is not responsible for the origin of UMR in oxidized Al/Cu bilayer films.

The role of the interface was investigated by measuring the dependence of the UMR on the thickness of the Al and Cu layers. Figure 4(c) shows $\Delta R_{xx}^{2\omega}$ as a function of the Al thickness measured at 300 K in oxidized Al(t_{Al} nm)/Cu(4 nm) bilayer films, where the thickness of the copper layer is kept at 4 nm to ensure that there is sufficiently thick copper to be oxidized when the aluminum layer is set at 1 nm. The curves exhibit an initial sharp increase below 3 nm followed by a gradual decrease to zero as the Al layer thickens. It was established in previous experiments that Cu undergoes oxidation when the Al layer thickness is below 8 nm [49]. Thus, the initial increase in UMR aligns with the rise in conductance in CuO_x.

Conversely, the signal attenuation in thicker Al samples is attributed to the reduction of CuO_x. The consistent, monotonic drop in the signal as the thickness of Cu films increases indicates that conduction is predominantly governed by the low resistivity of Cu in Fig. 4(d), with almost no proportion of the current experiencing scattering at the AlO_x/CuO_x interfacial region. These findings lead to the conclusion that the interface contribution is the dominant factor in determining the UMR effect. According to the above results, the scattering of the accumulated polarized electrons with the magnetic moment of CuO_x at the AlO_x/CuO_x interfacial region is responsible for the UMR effect, which was further confirmed by spin Hall magnetoresistance measurements (Appendix D).

VI. CONCLUSIONS

In summary, we experimentally observe a large UMR in naturally oxidized light-metal Al/Cu bilayer films even in the absence of an artificial ferromagnetic layer. Through the temperature and thickness dependence in oxidized Al/Cu bilayer and contrasting Al/Cu/Co trilayer films, the UMR mechanism of the interfacial scattering occurring between the magnetic moment of CuO_x and polarized electrons at the AlO_x/CuO_x interfacial region was determined. Our results demonstrate that the interfacial magnetic moment may play a crucial role even in the weak magnetization system to generate UMR. It will further motivate the development of UMR, using interface engineering.

ACKNOWLEDGMENTS

This work was supported by the National Natural Science Foundation of China (Grant No. 12074157), Gansu Key Research and Development Program under Grant No. 23YFGA0008, the 111 project (Grant No. B20063), and the Fundamental Research Funds for the Central Universities (Grant No. lzujbky-2022-kb06).

APPENDIX A: MAGNETIC MEASUREMENTS

The magnetic properties of the oxidized Al(2 nm)/Cu(4 nm) bilayer films were measured by a superconducting quantum interference device (SQUID). As shown in Fig. 5(a), it is magnetically very weak, displaying no discernible saturated magnetic moment even at 70 kOe and 300 K. Additionally, the magnetic moment demonstrates an upswing with decreasing temperature, as evidenced by zero-field cooling (ZFC) and field cooled (FC) measurements performed at 1 kOe, as shown in Fig. 5(b), which is similar to the observation in small CuO nanoparticles [56]. For the oxidized Al(2 nm)/Cu(4 nm) bilayer films, the ZFC-FC curves manifest a bifurcation at approximately 220 K, signifying the emergence of long-range magnetic order.

Given that the weak ferromagnetic response originated from the CuO_x layer, it is judicious to normalize the magnetization with respect to the surface area of the substrate (5×4.5 mm^2) instead of the volume of the CuO_x film. The weak ferromagnetism in oxidized Al(2 nm)/Cu(4 nm)

bilayer films resembles recent findings on 3-nm-thick naturally oxidized Cu thin films in Si/SiO_2 substrate [48]. Furthermore, we found that the ZFC-FC bifurcation point coincides with the Néel temperature of the CuO nanoscale particles, indicative of antiferromagnetic couplings at lower temperatures [56].

In addition, the hysteresis loop was characterized in Al(3 nm)/Cu(1.6 nm)/Co(3 nm) trilayer films as shown in Fig. 5(c). It was observed that the magnetic moment of the Co layer reached saturation at a magnetic field strength of 50 Oe. This indicates that the UMR at low field originates from the Cu/Co interface.

APPENDIX B: SHUNTING EFFECT IN OXIDIZED Al/Cu AND Al/Cu/Co HETEROSTRUCTURES

We conducted a systematic analysis of the resistance in oxidized Al(t_{Al} nm)/Cu(4 nm) bilayer films, as illustrated in Fig. 6(a). For Al thicknesses below 4 nm, we observe no significant change in resistance under identical test conditions, as depicted in Fig. 6(b). This suggests nearly complete oxidation of Al, and the corresponding equivalent circuit is presented in Fig. 6(c). As the Al layer thickness exceeds 8 nm, net Al starts to emerge, leading to a transition in the equivalent circuit from Fig. 6(c) to Fig. 6(d). Notably, the equivalent circuit for oxidized Al(3 nm)/Cu(t_{Cu} nm) bilayer films aligns with Fig. 6(c).

We initially assume that the film's resistance comprises two independent resistors in parallel. The first resistor represents the combined resistance of the CuO_x layer and the AlO_x/CuO_x interface, demonstrating UMR. The second resistor corresponds to the resistance of the Cu layers, which remains independent of the current. Consequently, we use the expanded model of the Fuchs-Sondheimer theory to estimate the resistivity of each layer [57]. This model, previously applied to a Bi/Ag/CoFeB system [58], describes the reciprocal of electrical resistance as follows:

$$\begin{aligned}\frac{1}{R_{xx}} &= \frac{1}{R_{AlO_x/CuO_x}} + \frac{1}{R_{CuO_x}} + \frac{1}{R_{Cu}} \\ &= \frac{1}{R_{AlO_x/CuO_x}} + \frac{1}{R_{CuO_x}} \\ &\quad + \frac{w(t_{Cu}-h)}{\rho_{Cu}^{\infty} l\left[1+\frac{3}{8(t_{Cu}-h)}(1-p)l_{Cu}^{\infty}\right]}.\end{aligned} \tag{B1}$$

Here R_{AlO_x/CuO_x}, R_{CuO_x}, and R_{Cu} are the resistances of the AlO_x/CuO_x interface, CuO_x layer, and Cu layer, respectively; ρ_{Cu}^{∞} and l_{Cu}^{∞} are the resistivity and the mean free path for an infinitely thick Cu film, respectively; ρ is the scattering parameter at the interfaces; h is the parameter for the surface roughness amplitude; and w/l is set to 1/8. The equation is well fitted to the data in Fig. 6(e). The fitted results $\rho_{Cu}^{\infty} = 3.8\ \mu\Omega$ cm and $l_{Cu}^{\infty} = 39$ nm, closely match the reported values of 1.75 $\mu\Omega$ cm and 39 nm, where $p = 0.3$ and $h = 1.0$ nm. The sum of the fitted resistances of the AlO_x/CuO_x interface and the CuO_x layer is 1695 Ω. In this parallel circuit, the normalized UMR is written as

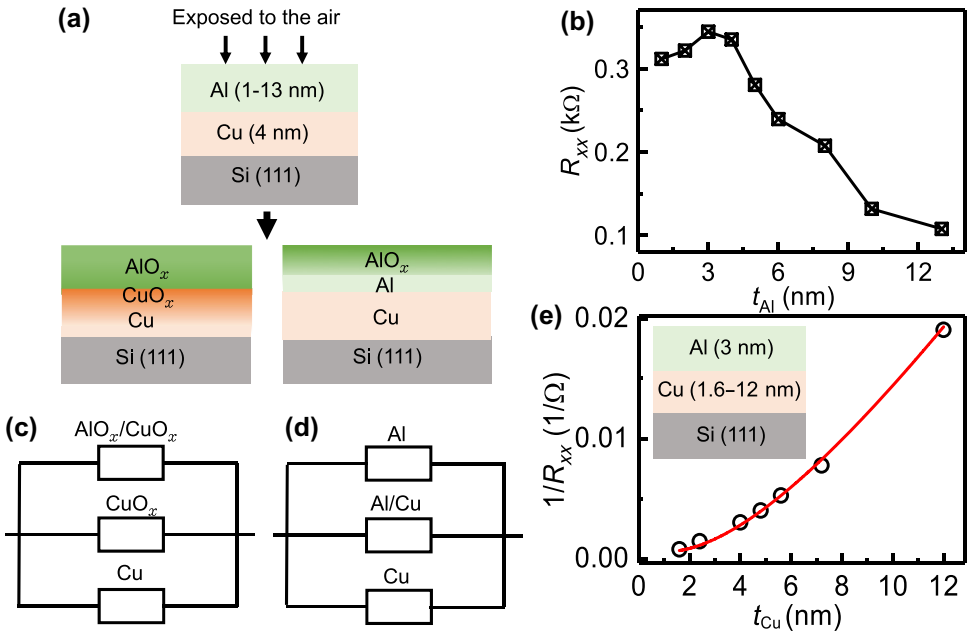

FIG. 6. (a) Schematics of the oxidized Al/Cu bilayer films. (b) The corresponding resistance of the Al(t_{Al} nm)/Cu(4 nm) bilayer films as a function of t_{Al}. (c),(d) The equivalent circuits for the oxidized Al/Cu bilayer films. (e) The reciprocal of sheet resistance ($1/R_{xx}$) of the Al(3 nm)/Cu(t_{Cu} nm) bilayer films as a function of t_{Cu} at 300 K.

follows [58]:

$$\frac{R^{\mathrm{UMR}}}{R_{xx}} = R_{xx}\frac{R^{\mathrm{UMR}}}{[1/(1/R_{\mathrm{AlO}_x/\mathrm{CuO}_x} + 1/R_{\mathrm{CuO}_x})]^2} = 0.073\%.$$

The shunting effect in oxidized Al(3 nm)/Cu(1.6 nm)/Co(3 nm) trilayer films was also analyzed. The resistance of the oxidized Al(3 nm)/Cu(1.6 nm)/Co(3 nm) trilayer films is measured to be 380 Ω at room temperature, while the resistance of the naturally oxidized Al(3 nm)/Cu(1.6 nm) sample is 1297 Ω under the same Hall bar aspect-ratio condition. Applying the parallel resistance model, the longitudinal resistance of the Co layer and the CuO_x/Co interface is estimated to be approximately 537.65 Ω. The corresponding current through the oxidized Al/Cu bilayer films decreases by a factor of 3.41, leading to a 3.41-fold reduction in $\Delta R_{xx}^{2\omega}$. Considering positive $\Delta R_{xx}^{2\omega}$ in the CuO_x/Co structure (including the CuO_x/Co interface and the Co layer), the calculated $\Delta R_{xx}^{2\omega}$ is 77.95 mΩ in Al(3 nm)/Cu(1.6 nm)/Co(3 nm) trilayer films and 112.85 mΩ in Al(3 nm)/Cu(1.6 nm) bilayer films at $j = 1.46 \times 10^7$ A/cm^2 and $H = 90$ kOe [Fig. 1(d)]. Obviously, $\Delta R_{xx}^{2\omega}$ in the trilayer films is slightly (1.4 times) smaller than in the bilayer films. This difference may arise from the overestimation of the resistance of the Cu layer in the trilayer films due to the better crystal quality of the Cu on Co.

APPENDIX C: ST-FMR MEASUREMENTS

The temperature dependence of the efficiency of the generating polarized angular momentum at the oxidized Al/Cu interface was assessed by using the spin torque ferromagnetic resonance technique at different temperatures [59–61]. As shown in Fig. 7(a)–7(c), the ST-FMR spectra show typical resonance peaks in the frequency range of 8–12 GHz. It can be well fitted by the following equation [62,63]:

$$V = V_S\frac{\Delta H^2}{\Delta H^2 + (H - H_0)^2} + V_A\frac{\Delta H(H - H_0)}{\Delta H^2 + (H - H_0)^2}. \tag{C1}$$

Here H_0 (ΔH) is the resonance field (resonance linewidth); and V_S and V_A are the symmetric and antisymmetric Lorentzian coefficients, which mainly arise from damping-like torque and field-like torque.

As expected from the aforementioned equation, the resonance peak shapes follow the sum of symmetric and antisymmetric Lorentzian curves, an example of which for 10 GHz is shown in Fig. 7(d). By fitting the ST-FMR spectra at different temperatures, V_S and V_A as functions of temperature were obtained. It is found in Fig. 7(e) that V_S is almost constant. However, the absolute value of V_A monotonically decreases with temperature from 300 to 100 K,

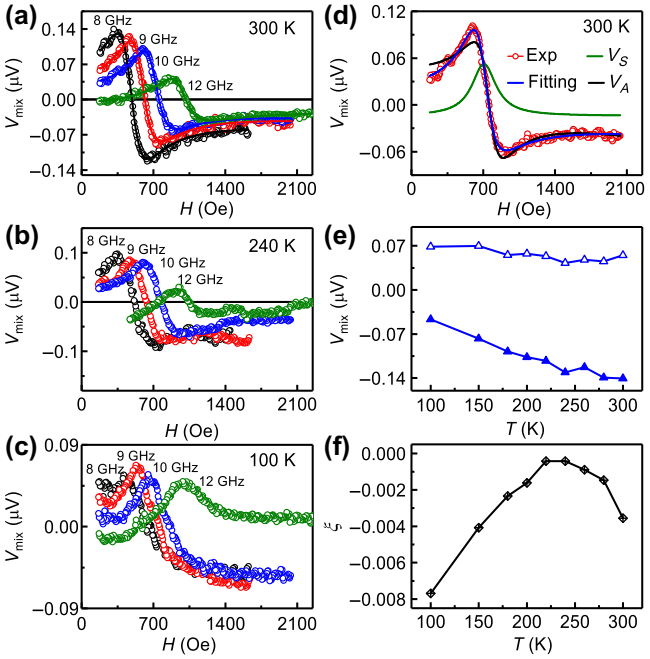

FIG. 7. (a)–(c) The ST-FMR spectrum of the Al(3 nm)/Cu(1.6 nm)/Co(3 nm) sample at (a) 300 K, (b) 240 K, and (c) 100 K. (d) Fitted result by (B1) for raw data. Circles are measured data; green, black, and blue lines are, respectively, symmetric and antisymmetric components and the sum of the raw data. (e) Summaries of symmetric V_S (open triangles) and antisymmetric V_A (filled triangles) as functions of temperature at 10 GHz microwave frequency. (f) The charge-spin conversion efficiency ξ as a function of temperature.

which may stem from the competition between Oersted field and field-like effective field in the sample.

Furthermore, the quantitative charge-spin conversion efficiency ξ can be determined by the following equation:

$$\xi = \frac{V_S}{V_A}\frac{e\mu_0 M_s t_{\mathrm{Co}} d_{\mathrm{CuO}_x}}{\hbar}\left(1 + \frac{M_s}{H_0}\right)^{1/2}, \tag{C2}$$

where t_{Co} and d_{CuO_x} are the thicknesses of Co and CuO_x, respectively, and M_s is the effective saturation magnetization. Figure 7(f) reports ξ as a function of temperature T. Upon increasing temperature, ξ decreases from 0.0077 at 100 K to a minimum 0.00042 at 220 K, and then increases to 0.0036 at about 300 K. Below 200 K, the observed $\xi(T)$ remarkably increases with decreasing temperature, suggesting that the generation of polarized angular momentum is on the rise at lower temperatures. Additionally, we note that the spin Hall angle of 0.0036 for the oxidized Al/Cu/Co heterostructure at room temperature is lower compared to the reported value of 0.01 in CuO_x/Co(2.5 nm) bilayer films. This discrepancy might be attributed to the improved crystal quality of Co in our sample.

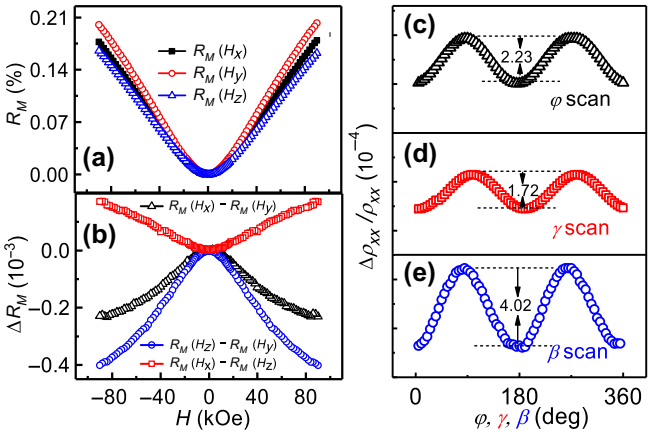

FIG. 8. (a) Magnetic-field-dependent magnetoresistance $R_M = [\rho_{xx}(H) - \rho_{xx}(H{=}0)]/\rho_{xx}(H{=}0)$ measured with the magnetic field applied in a plane parallel (x) and perpendicular (y) to the direction of the current and out of the plane perpendicular (z) to the direction of the current. (b) The R_M difference between the different directions. (c)–(e) Angle-dependent $\Delta\rho_{xx}/\rho_{xx} = [\rho_{xx}(\varphi,\gamma,\beta) - \rho_{xx}(\varphi,\gamma,\beta{=}0)]/\rho_{xx}(\varphi,\gamma,\beta{=}0)$ in the three rotation planes for the Al(3 nm)/Cu(1.6 nm) bilayer films. The magnetic field was set as 70 kOe and the applied charge current in the x direction of a Hall bar structure is 1 mA.

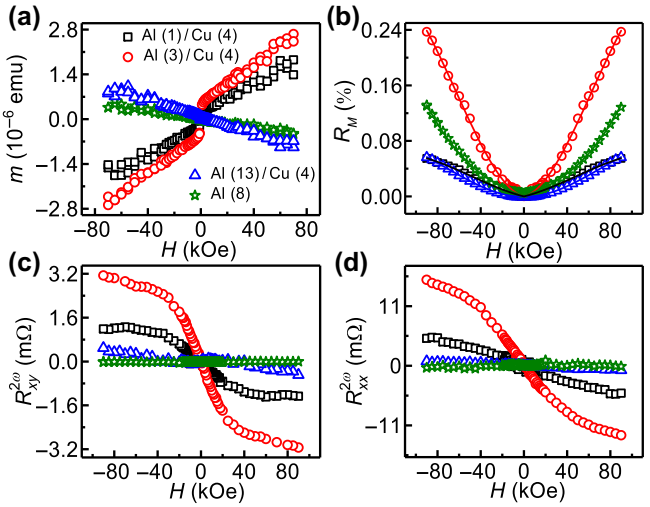

FIG. 9. (a) The m vs H curve of the oxidized Al/Cu bilayer and Al single films in an in-plane H configuration on Si substrate. (b) Magnetic field H dependence of the first-harmonic longitudinal magnetoresistance. (c),(d) The second-harmonic transverse resistance $R_{xy}^{2\omega}$ (c) and longitudinal resistance $R_{xx}^{2\omega}$ (d) as functions of H.

APPENDIX D: SPIN HALL MAGNETORESISTANCE IN OXIDIZED Al/Cu BILAYER FILMS

In addition to UMR, spin Hall magnetoresistance is another method for detecting interactions between polarized currents (spin or orbital currents) and weak magnetic moments. The absorption of polarized currents by the magnetic layer is contingent upon the magnetization (M) direction. Unabsorbed polarized currents are then reflected and converted into in-plane charge currents, resulting in an SMR [$R_M(m{=}z) \neq R_M(m{=}y)$]. The longitudinal magnetoresistance (R_M) of the Al(3 nm)/Cu(1.6 nm) sample was measured at 300 K, as depicted in Fig. 8(a), with field orientations along the x, y, and z axes defined as H_x, H_y, and H_z, respectively.

A noticeable difference was observed between $R_M(H_y)$ and $R_M(H_z)$ [i.e., $\Delta R_M = R_M(H_z) - R_M(H_y)$] as illustrated in Fig. 8(b), with $\Delta R_M < 0$, indicating the presence of negative SMR. This is similar to the reported negative SMR in Ta/NiFe bilayer films [64]. This finding was substantiated by angle-dependent $\Delta\rho_{xx}/\rho_{xx}$ measurements, as shown in Figs. 8(c)–8(e). Notably, $\Delta\rho_{xx}/\rho_{xx}$ exhibits a second-order cosine symmetric R_M in the $y0z$ plane perpendicular to the current direction, as depicted in Fig. 8(e).

APPENDIX E: MAGNETIC ORIGIN

To exclude the possibility that the weak ferromagnetic behavior in oxidized Al/Cu bilayer films originates from contaminants or defects in other layers, we conducted separate measurements, including m vs H, R vs H, $R_{xy}^{2\omega}$, and $R_{xx}^{2\omega}$, for Cu films with different degrees of oxidation and single Al films. It can be observed that, with an increase in Al thickness from 1 to 13 nm, accompanied by the transition of Cu from an oxidized state to an unoxidized state, the m vs H curves show a transition from weak ferromagnetism to diamagnetism, as illustrated in Fig. 9(a). To further eliminate the influence of the silicon substrate and the Al layer, we grew 8 nm of Al on the silicon surface. This copper-free sample also exhibits diamagnetism in the m vs H curve.

Both results indicate that the weak ferromagnetic signal arises from Cu oxidation. In the magnetoresistance test [Fig. 9(b)], when Al is at 8 and 13 nm, R_M conforms to H^2, indicating the dominant factor of the Lorentz force. Figures 9(c) and 9(d) show $R_{xy}^{2\omega}$ and $R_{xx}^{2\omega}$ with varying Al thickness. For the Al(13 nm)/Cu(4 nm) and Al(8 nm) samples, no significant $R_{xy}^{2\omega}$ and $R_{xx}^{2\omega}$ signals were observed. However, when the Al thickness is reduced to 1 and 3 nm, both $R_{xy}^{2\omega}$ and $R_{xx}^{2\omega}$ exhibit a notable increase with the magnetic field. These results suggest that the emergence of magnetism is attributed to the oxidation of copper.

APPENDIX F: UMR IN OXIDIZED Ta/Cu BILAYER FILMS

To confirm that the observed UMR in the samples indeed originates from the oxidation of Cu, we initially grew a 4-nm-thick Cu film on a Si(111) substrate using molecular beam epitaxy. Subsequently, *ex situ* magnetron

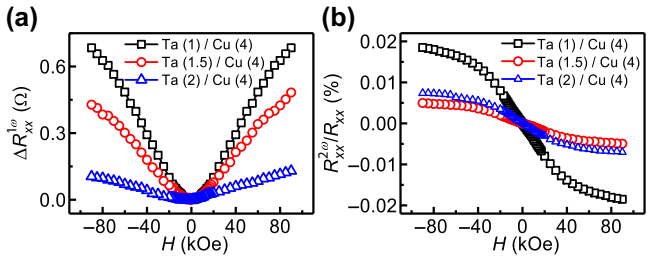

FIG. 10. (a) Magnetic field H dependence of the magnitude of the first-harmonic longitudinal resistance $\Delta R_{xx}^{1\omega}$ in oxidized Ta(t_{Ta} nm)/Cu(4 nm) heterostructures recorded at $I = 4$ mA. (b) The ratio of the second-harmonic to the first-harmonic resistance $\Delta R_{xx}^{2\omega}/R_{xx}^{1\omega}$ as a function of H.

sputtering was employed to grow 1-, 1.5-, and 2-nm-thick Ta films on the surface of Cu. For transport measurements, these were fashioned into Hall bars with an aspect ratio of 8. Experimental results similar to those in oxidized Al/Cu films were observed, as shown in Figs. 10(a) and 10(b).

[1] W. P. Sterk, D. Peerlings, and R. A. Duine, Magnon contribution to unidirectional spin Hall magnetoresistance in ferromagnetic-insulator/heavy-metal bilayers, Phys. Rev. B **99**, 064438 (2019).

[2] C. O. Avci, J. Mendil, G. S. D. Beach, and P. Gambardella, Origins of the unidirectional spin hall magnetoresistance in metallic bilayers, Phys. Rev. Lett. **121**, 087207 (2018).

[3] J. Železný, Z. Fang, K. Olejník, J. Patchett, F. Gerhard, C. Gould, L. W. Molenkamp, C. Gomez-Olivella, J. Zemen, T. Tichý, T. Jungwirth, and C. Ciccarelli, Unidirectional magnetoresistance and spin-orbit torque in NiMnSb, Phys. Rev. B **104**, 054429 (2021).

[4] T. Ideue, K. Hamamoto, S. Koshikawa, M. Ezawa, S. Shimizu, Y. Kaneko, Y. Tokura, N. Nagaosa, and Y. Iwasa, Bulk rectification effect in a polar semiconductor, Nat. Phys. **13**, 578 (2017).

[5] Y. Tokura and N. Nagaosa, Nonreciprocal responses from non-centrosymmetric quantum materials, Nat. Commun. **9**, 3740 (2018).

[6] Y. Lv, J. Kally, D. Zhang, J. S. Lee, M. Jamali, N. Samarth, and J.-P. Wang, Unidirectional spin-Hall and Rashba-Edelstein magnetoresistance in topological insulator-ferromagnet layer heterostructures, Nat. Commun. **9**, 111 (2018).

[7] Y. Miao, D. Yang, L. Jia, X. Li, S. Yang, C. Gao, and D. Xue, Magnetocrystalline anisotropy correlated negative anisotropic magnetoresistance in epitaxial $Fe_{30}Co_{70}$ thin films, Appl. Phys. Lett. **118**, 042404 (2021).

[8] J. Kim, P. Sheng, S. Takahashi, S. Mitani, and M. Hayashi, Spin hall magnetoresistance in metallic bilayers, Phys. Rev. Lett. **116**, 097201 (2016).

[9] H. Nakayama, M. Althammer, Y.-T. Chen, K. Uchida, Y. Kajiwara, D. Kikuchi, T. Ohtani, S. Geprägs, M. Opel, S. Takahashi, R. Gross, G. E. W. Bauer, S. T. B. Goennenwein, and E. Saitoh, Spin hall magnetoresistance induced by a nonequilibrium proximity effect, Phys. Rev. Lett. **110**, 206601 (2013).

[10] C. O. Avci, K. Garello, A. Ghosh, M. Gabureac, S. F. Alvarado, and P. Gambardella, Unidirectional spin Hall magnetoresistance in ferromagnet/normal metal bilayers, Nat. Phys. **11**, 570 (2015).

[11] S. Sun, B. Wang, W. Li, X. Zeng, Y. Guo, B. Han, T. Wang, D. Yang, X. Fan, and J. Cao, Coexistence of spin-orbit torque and unidirectional magnetoresistance effect induced by spin polarization with spin rotation symmetry in Co/Cu/Co structures, Phys. Rev. B **106**, 094422 (2022).

[12] K. Yamanoi, H. Semizu, and Y. Nozaki, Enhancement of room-temperature unidirectional spin Hall magnetoresistance by using a ferromagnetic metal with a low Curie temperature, Phys. Rev. B **106**, L140401 (2022).

[13] S. Wang, X. Cui, R. Xie, C. Zhang, Y. Tian, L. Bai, Q. Huang, Q. Cao, and S. Yan, Controllable unidirectional magnetoresistance in ferromagnetic films with broken symmetry, Phys. Rev. B **107**, 094410 (2023).

[14] J. H. Lee, T. Harada, F. Trier, L. Marcano, F. Godel, S. Valencia, A. Tsukazaki, and M. Bibes, Nonreciprocal transport in a Rashba ferromagnet, delafossite $PdCoO_2$, Nano Lett. **21**, 8687 (2021).

[15] K. Hasegawa, T. Koyama, and D. Chiba, Enhanced unidirectional spin Hall magnetoresistance in a Pt/Co system with a Cu interlayer, Phys. Rev. B **103**, L020411 (2021).

[16] X. Zhou, F. Zeng, M. Jia, H. Chen, and Y. Wu, Sign reversal of unidirectional magnetoresistance in monocrystalline Fe/Pt bilayers, Phys. Rev. B **104**, 184413 (2021).

[17] K. Lou, Q. Zhao, B. Jiang, and C. Bi, Large anomalous unidirectional magnetoresistance in a single ferromagnetic layer, Phys. Rev. Appl. **17**, 064052 (2022).

[18] T.-Y. Chang, C.-L. Cheng, C.-C. Huang, C.-W. Peng, Y.-H. Huang, T.-Y. Chen, Y.-T. Liu, and C.-F. Pai, Large unidirectional magnetoresistance in metallic heterostructures in the spin transfer torque regime, Phys. Rev. B **104**, 024432 (2021).

[19] L. Chen, K. Zollner, S. Parzefall, J. Schmitt, M. Kronseder, J. Fabian, D. Weiss, and C. H. Back, Connections between spin-orbit torques and unidirectional magnetoresistance in ferromagnetic-metal–heavy-metal heterostructures, Phys. Rev. B **105**, L020406 (2022).

[20] C. Lidig, J. Cramer, L. Weißhoff, T. Thomas, T. Kessler, M. Kläui, and M. Jourdan, Unidirectional spin Hall magnetoresistance as a tool for probing the interfacial spin polarization of Co_2MnSi, Phys. Rev. Appl. **11**, 044039 (2019).

[21] S. S.-L. Zhang and G. Vignale, Theory of unidirectional spin Hall magnetoresistance in heavy-metal/ferromagnetic-metal bilayers, Phys. Rev. B **94**, 140411(R) (2016).

[22] Y. Cheng, J. Tang, J. J. Michel, S. K. Chong, F. Yang, R. Cheng, and K. L. Wang, Unidirectional spin hall magnetoresistance in antiferromagnetic heterostructures, Phys. Rev. Lett. **130**, 086703 (2023).

[23] M. Akaike, Y. Nii, H. Masuda, and Y. Onose, Nonreciprocal electronic transport in $PdCrO_2$: Implication of spatial inversion symmetry breaking, Phys. Rev. B **103**, 184428 (2021).

[24] C. O. Avci, K. Garello, J. Mendil, A. Ghosh, N. Blasakis, M. Gabureac, M. Trassin, M. Fiebig, and P. Gambardella, Magnetoresistance of heavy and light metal/ferromagnet bilayers, Appl. Phys. Lett. **107**, 192405 (2015).

[25] I. V. Borisenko, V. E. Demidov, S. Urazhdin, A. B. Rinkevich, and S. O. Demokritov, Relation between unidirectional spin Hall magnetoresistance and spin current-driven magnon generation, Appl. Phys. Lett. **113**, 062403 (2018).
[26] Y. Yin, D.-S. Han, M. C. H. de Jong, R. Lavrijsen, R. A. Duine, H. J. M. Swagten, and B. Koopmans, Thickness dependence of unidirectional spin-Hall magnetoresistance in metallic bilayers, Appl. Phys. Lett. **111**, 232405 (2017).
[27] D. C. Vaz, F. Trier, A. Dyrdał, A. Johansson, K. Garcia, A. Barthélémy, I. Mertig, J. Barnaś, A. Fert, and M. Bibes, Determining the Rashba parameter from the bilinear magnetoresistance response in a two-dimensional electron gas, Phys. Rev. Mater. **4**, 071001(R) (2020).
[28] Y. Li, Y. Li, P. Li, B. Fang, X. Yang, Y. Wen, D. Zheng, C. Zhang, X. He, Z. C. Manchon, Aurélien Manchon, and X. Zhang, Nonreciprocal charge transport up to room temperature in bulk Rashba semiconductor α-GeTe, Nat. Commun. **12**, 540 (2021).
[29] K. Hamamoto, M. Ezawa, K. W. Kim, T. Morimoto, and N. Nagaosa, Nonlinear spin current generation in noncentrosymmetric spin-orbit coupled systems, Phys. Rev. B **95**, 224430 (2017).
[30] T. Guillet, C. Zucchetti, Q. Barbedienne, A. Marty, G. Isella, L. Cagnon, C. Vergnaud, H. Jaffrès, N. Reyren, J.-M. George, A. Fert, and M. Jamet, Observation of large unidirectional Rashba magnetoresistance in Ge(111), Phys. Rev. Lett. **124**, 027201 (2020).
[31] G. Okano, M. Matsuo, Y. Ohnuma, S. Maekawa, and Y. Nozaki, Nonreciprocal spin current generation in surface-oxidized copper films, Phys. Rev. Lett. **122**, 217701 (2019).
[32] S. Ding, P. Noël, G. K. Krishnaswamy, and P. Gambardella, Unidirectional orbital magnetoresistance in light-metal–ferromagnet bilayers, Phys. Rev. Res. **4**, L032041 (2022).
[33] N. Roschewsky, E. S. Walker, P. Gowtham, S. Muschinske, F. Hellman, S. R. Bank, and S. Salahuddin, Spin-orbit torque and Nernst effect in BiSb/Co heterostructures, Phys. Rev. B **99**, 195103 (2019).
[34] M. DC, R. Grassi, J.-Y. Chen, M. Jamali, D. Reifsnyder Hickey, D. Zhang, Z. Zhao, H. Li, P. Quarterman, Y. Lv, M. Li, A. Manchon, K. A. Mkhoyan, T. Low, and J.-P. Wang, Room-temperature high spin–orbit torque due to quantum confinement in sputtered Bi_xSe_{1-x} films, Nat. Mater. **17**, 800 (2018).
[35] P. Li, W. Wu, Y. Wen, C. Zhang, J. Zhang, S. Zhang, Z. Yu, S. A. Yang, A. Manchon, and X. Zhang, Spin-momentum locking and spin-orbit torques in magnetic nano-heterojunctions composed of Weyl semimetal WTe_2, Nat. Commun. **9**, 800 (2018).
[36] T. H. Pham, S.-G. Je, P. Vallobra, T. Fache, D. Lacour, G. Malinowski, M. C. Cyrille, G. Gaudin, O. Boulle, M. Hehn, J.-C. Rojas-Sánchez, and S. Mangin, Thermal contribution to the spin-orbit torque in metallic-ferrimagnetic systems, Phys. Rev. Appl. **9**, 064032 (2018).
[37] S. S. Li and T. Rabson, The Nernst and the Seebeck effects in Te-doped BiSb alloys, Solid-State Electron. **13**, 153 (1970).
[38] C. O. Avci, K. Garello, M. Gabureac, A. Ghosh, A. Fuhrer, S. F. Alvarado, and P. Gambardella, Interplay of spin-orbit torque and thermoelectric effects in ferromagnet/normal-metal bilayers, Phys. Rev. B **90**, 224427 (2014).
[39] M. Schreier, N. Roschewsky, E. Dobler, S. Meyer, H. Huebl, R. Gross, and S. T. B. Goennenwein, Current heating induced spin Seebeck effect, Appl. Phys. Lett. **103**, 242404 (2013).
[40] S. Ding, A. Ross, D. Go, L. Baldrati, Z. Ren, F. Freimuth, S. Becker, F. Kammerbauer, J. Yang, G. Jakob, Y. Mokrousov, and M. Kläui, Harnessing orbital-to-spin conversion of interfacial orbital currents for efficient spin-orbit torques, Phys. Rev. Lett. **125**, 177201 (2020).
[41] D. Go, D. Jo, T. Gao, K. Ando, S. Blügel, H.-W. Lee, and Y. Mokrousov, Orbital Rashba effect in a surface-oxidized Cu film, Phys. Rev. B **103**, L121113 (2021).
[42] J. Kim, D. Go, H. Tsai, D. Jo, K. Kondou, H.-W. Lee, and Y. Otani, Nontrivial torque generation by orbital angular momentum injection in ferromagnetic-metal/Cu/Al_2O_3 trilayers, Phys. Rev. B **103**, L020407 (2021).
[43] Y. Kageyama, Y. Tazaki, H. An, T. Harumoto, T. Gao, J. Shi, and K. Ando, Spin-orbit torque manipulated by fine-tuning of oxygen-induced orbital hybridization, Sci. Adv. **5**, eaax4278 (2019).
[44] H. An, Y. Kageyama, Y. Kanno, N. Enishi, and K. Ando, Spin torque generator engineered by natural oxidation of Cu, Nat. Commun. **7**, 13069 (2016).
[45] T. Gao, A. Qaiumzadeh, H. An, A. Musha, Y. Kageyama, J. Shi, and K. Ando, Intrinsic spin-orbit torque arising from the berry curvature in a metallic-magnet/Cu-oxide interface, Phys. Rev. Lett. **121**, 017202 (2018).
[46] T. An, B. Cui, L. Liu, M. Zhang, F. Liu, W. Liu, J. Xie, X. Ren, R. Chu, B. Cheng, C. Jiang, and J. Hu, Enhanced spin current in $Ni_{81}Fe_{19}$/Cu–CuO_x bilayer with top and sideways oxidization, Adv. Mater. **35**, 2207988 (2023).
[47] T. An, B. Cui, M. Zhang, F. Liu, S. Cheng, K. Zhang, X. Ren, L. Liu, B. Cheng, C. Jiang, and J. Hu, Electrical manipulation of orbital current via oxygen migration in $Ni_{81}Fe_{19}$/Cu–CuO_x/TaN heterostructure, Adv. Mater. **n/a**, 2300858 (2023).
[48] J. Jiang, W. Zhao, F. Wang, R. Du, L. Miao, K. Wang, Q. Li, C.-Z. Chang, and M. H. W. Chan, Long-range superconducting proximity effect in nickel nanowires, Phys. Rev. Res. **4**, 023133 (2022).
[49] L. Zhao, Y. Li, Y. Wang, P. Chen, B. Lv, and C. Gao, Anomalous Hall effect in naturally oxidized normal-metal Al/Cu double films, J. Phys. D: Appl. Phys. **57**, 055302 (2024).
[50] A. B. Pippard, *Magnetoresistance in Metals* (Cambridge University Press, New York, 1989), Vol. 2.
[51] Y. Fan, P. Zhang, J. Han, Y. Lv, L. Liu, and J.-P. Wang, Observation of the unidirectional magnetoresistance in antiferromagnetic insulator Fe_2O_3/Pt bilayers, Adv. Electron. Mater. **9**, 2300232 (2023).
[52] S. Shim, M. Mehraeen, J. Sklenar, J. Oh, J. Gibbons, H. Saglam, A. Hoffmann, S. S.-L. Zhang, and N. Mason, Unidirectional magnetoresistance in antiferromagnet/heavy-metal bilayers, Phys. Rev. X **12**, 021069 (2022).
[53] N. H. Duy Khang and P. N. Hai, Giant unidirectional spin Hall magnetoresistance in topological insulator–ferromagnetic semiconductor heterostructures, J. Appl. Phys. **126**, 233903 (2019).

[54] K. Yasuda, A. Tsukazaki, R. Yoshimi, K. S. Takahashi, M. Kawasaki, and Y. Tokura, Large unidirectional magnetoresistance in a magnetic topological insulator, Phys. Rev. Lett. **117**, 127202 (2016).

[55] Y. Tazaki, Y. Kageyama, H. Hayashi, T. Harumoto, T. Gao, J. Shi, and K. Ando, Current-induced torque originating from orbital current, arXiv:2004.09165.

[56] A. Punnoose, H. Magnone, M. S. Seehra, and J. Bonevich, Bulk to nanoscale magnetism and exchange bias in CuO nanoparticles, Phys. Rev. B **64**, 174420 (2001).

[57] K. Fuchs, The conductivity of thin metallic films according to the electron theory of metals, Math. Proc. Camb. Philos. Soc. **34**, 100 (1938).

[58] H. Nakayama, Y. Kanno, H. An, T. Tashiro, S. Haku, A. Nomura, and K. Ando, Rashba-Edelstein magnetoresistance in metallic heterostructures, Phys. Rev. Lett. **117**, 116602 (2016).

[59] N. Mecking, Y. S. Gui, and C.-M. Hu, Microwave photovoltage and photoresistance effects in ferromagnetic microstrips, Phys. Rev. B **76**, 224430 (2007).

[60] L. Liu, T. Moriyama, D. C. Ralph, and R. A. Buhrman, Spin-torque ferromagnetic resonance induced by the spin hall effect, Phys. Rev. Lett. **106**, 036601 (2011).

[61] W. Kong, X. Fan, H. Zhou, J. Cao, D. Guo, Y. S. Gui, C.-M. Hu, and D. Xue, Electrical detection of magnetization dynamics in an ultrathin CoFeB film with perpendicular anisotropy, Appl. Phys. Lett. **109**, 182406 (2016).

[62] Y. Cui, X. Feng, Q. Zhang, H. Zhou, W. Jiang, J. Cao, D. Xue, and X. Fan, Absence of spin Hall magnetoresistance in Pt/$(CoNi)_n$ multilayers, Phys. Rev. B **103**, 024415 (2021).

[63] H. Bai, X. F. Zhou, H. W. Zhang, W. W. Kong, L. Y. Liao, X. Y. Feng, X. Z. Chen, Y. F. You, Y. J. Zhou, L. Han, W. X. Zhu, F. Pan, X. L. Fan, and C. Song, Control of spin-orbit torques through magnetic symmetry in differently oriented noncollinear antiferromagnetic Mn_3Pt, Phys. Rev. B **104**, 104401 (2021).

[64] M.-G. Kang, G. Go, K.-W. Kim, J.-G. Choi, B.-G. Park, and K.-J. Lee, Negative spin Hall magnetoresistance of normal metal/ferromagnet bilayers, Nat. Commun. **11**, 1 (2020).